Physica Scripta



# A new quench detection method for HTS magnets: stray-capacitance change monitoring

OPEN ACCESS
IOP Publishing
Physica Scripta
Phys. Scr. **95** (2020) 015002 (12pp)
https://doi.org/10.1088/1402-4896/ab4570

# A new quench detection method for HTS magnets: stray-capacitance change monitoring

**E Ravaioli[1,2], D Davis[1,3], M Marchevsky[1], GL Sabbi[1], T Shen[1], A Verweij[2] and K Zhang[1,4]**

[1] Lawrence Berkeley National Laboratory, Berkeley, CA, United States of America
[2] CERN, Geneva, CH, Switzerland
[3] NHMFL, Tallahassee, FL, United States of America
[4] Paul Scherrer Institut, Villigen, CH, Switzerland

E-mail: Emmanuale.Ravaioli@cern.ch

Received 2 April 2019, revised 5 August 2019
Accepted for publication 17 September 2019
Published 4 December 2019

**Abstract**

Fast quench detection is a key requirement for the successful implementation of superconducting magnet technology. In high temperature superconductor magnets, this issue is especially challenging due to the low quench propagation velocity, and presently represents one of the main factors limiting their application. A new detection technique based on stray-capacitance monitoring is proposed. The capacitance between electrically-insulated magnet elements, such as magnet structure and end parts, is utilized as an indication of local heat deposition in the conductor. In fact, the relative permittivity of helium drops when it changes from the liquid to the gaseous phase. Thus, when heating occurs, part of the helium impregnating the insulation layers boils off, and the monitored stray-capacitance decreases. The proposed technique is successfully demonstrated on three small-scale Bi-2212 magnets manufactured at the Lawrence Berkeley National Laboratory. Results from the detection of thermal runaways and spot-heater induced quenches are reported and discussed. Advantages and limitations of the stray-capacitance method with respect to conventional quench detection methods are assessed.

Keywords: accelerator magnet, high temperature superconductor, quench detection, quench protection, superconducting coil

(Some figures may appear in colour only in the online journal)

## 1. Introduction

Early detection of the quench development is critical for the protection of superconducting magnets. In many practical applications, high-energy density superconducting coils are damaged due to hot-spot overheating if active protection is not timely activated. The most common method for detecting the occurrence of a resistive transition in a low-temperature superconducting coil is voltage monitoring by means of dedicated taps [1, 2].

Fast quench detection in high-temperature superconductor (HTS) magnets is more challenging due to the very low normal zone propagation velocity [3–5]. This feature is one of the factors currently limiting wider application of HTS magnets. For this reason, various alternative quench detection methods have been explored in the past. These attempts include systems monitoring the voltage across coils magnetically coupled to the protected coil [6, 7], mechanical vibrations [8–13], local variations of magnetization and current distribution [14–20], variation of fiber refraction index with temperature [21–27], or voltage across non-contact capacitive sensors [28, 29].

Recently, we proposed a novel detection method based on monitoring the stray capacitances between magnet-structure elements [30]. The technique was successfully tested on a small-scale, race-track, $Ag/Bi_2Sr_2CaCu_2O_x$ (Bi-2212) magnet manufactured at the Lawrence Berkeley National Laboratory (LBNL) [31]. In this work, we describe in more detail the principles upon which the technique is based and present results from its implementation on two additional magnets, with the aim of further demonstrating and characterizing the proposed method [31, 32].

Magnets often include several metallic elements separated from the coil and from each other by layers of insulation material. Parts of the mechanical structures, supports around which the conductor is wound, and coil-end pieces are examples of such elements. During the transients preceding and following a quench, a number of effects occur, which affect the stray capacitances between the elements and the coil, and between each other. These include:

- local heat deposition, which increases the conductor temperature and causes thermal expansion;
- temperature increase, which affects the insulation material's relative permittivity;
- local changes of temperature, pressure, density, and state of the cryogenic fluid impregnating the insulation layers, which results in a change of its relative permittivity;
- sudden mechanical movements, which can alter the geometry of the coil and the magnet's metallic elements.

The proposed capacitance monitoring technique was implemented on three small-scale, race-track, Bi-2212 magnets manufactured at LBNL [31, 32]. The coils have the same geometry, but different conductor performances and impregnation schemes. The measurement setup and the experimental results will be described and discussed. Furthermore, advantages and limitations of this method will be assessed.

## 2. Method

The electrical capacitance between two elements is defined as $C = q/U$ (F), where $\pm q$ (C) is the electrical charge on the elements, and $U$ (V) the voltage across them. Calculations of $C$ for various geometries have been performed and are available in the literature [33]. Asimple example is the capacitance between two plane conductors, which is computed as $C = \epsilon_0\epsilon_r S/d$, where $\epsilon_0 \approx 8.854 \times 10^{-12}$ F m$^{-1}$ is the electric constant, $\epsilon_r$ the relative permittivity of the material between the conductors, $S$ (m$^2$) their contact surface, and $d$ (m) the distance between them.

In a superconducting magnet, mechanical, thermal, electrical, and fluid dynamic effects influence $C$ during the transients leading and following a quench. Local conductor heating causes the coil to expand against its structure, whose temperature and dimensions remain almost unaltered during the initial quench development. As a result, the insulation layers between the magnet elements are squeezed, hence reducing $d$ and increasing $C$. However, no significant size changes are expected for temperatures below about 30 K.

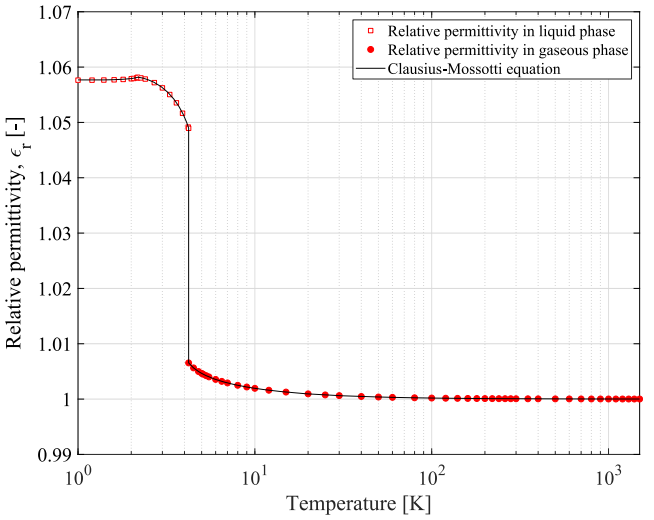


**Figure 1.** Relative permittivity of helium, measured at atmospheric pressure in liquid and gaseous phases, reported in [34]. The measured permittivity is compared to values calculated with the Clausius–Mossotti equation [34, 36, 37].

Therefore, it is unlikely to observe significant $C$ change due to thermal expansion at the early stage of the quench.

Relative permittivities of the insulation layers and of the cryogenic fluid impregnating them vary with temperature and fluid dynamic conditions. In particular, both helium's and nitrogen's $\epsilon_r$ slightly decrease with temperature when in liquid phase, and sharply decrease when their phase changes from liquid to gaseous [34, 35]. When heat is locally generated, part or all of the fluid trapped in the insulation layers evaporates, therefore causing a reduction of $\epsilon_r$ and consequently $C$.

Experimental values of helium $\epsilon_r$ at atmospheric pressure, available in the literature [34], are shown in figure 1. At a temperature of 4.222 K, helium is transferred from the liquid to the gaseous phase and its $\epsilon_r$ drops by about 4%. As shown in figure 1, this is consistent with the Clausius–Mossotti equation, which relates the relative permittivity of a fluid to its density [36, 37]:

$$\frac{3M}{4\pi}\frac{\epsilon_r - 1}{\epsilon_r + 2}\frac{1}{\rho} = p, \tag{1}$$

where $M$ (g mol$^{-1}$) is the fluid molar mass, $\rho$ (kg m$^{-3}$) its density, and $p$ (m$^3$ kg$^{-1}$) its specific polarizability. For helium, $M \approx 4.003 \times 10^{-3}$ kg mol$^{-1}$ and $p \approx A + B\rho$, with $A = 123.493 \times 10^{-6}$ m$^3$ kg$^{-1}$ and $B = -5.86 \times 10^{-9}$ m$^6$ kg$^{-2}$ [34].

This property can be exploited to detect early heat deposition, which can lead to a quench. Local heat deposition can cause the helium trapped in the insulation layers to evaporate. The local drop of its density causes a reduction of its $\epsilon_r$, and a consequent reduction of the monitored $C$.

## 3. Experimental setup

A series of tests were performed on three small-scale HTS magnets to evaluate the effectiveness of the proposed $C$ monitoring method. The three magnets are made of

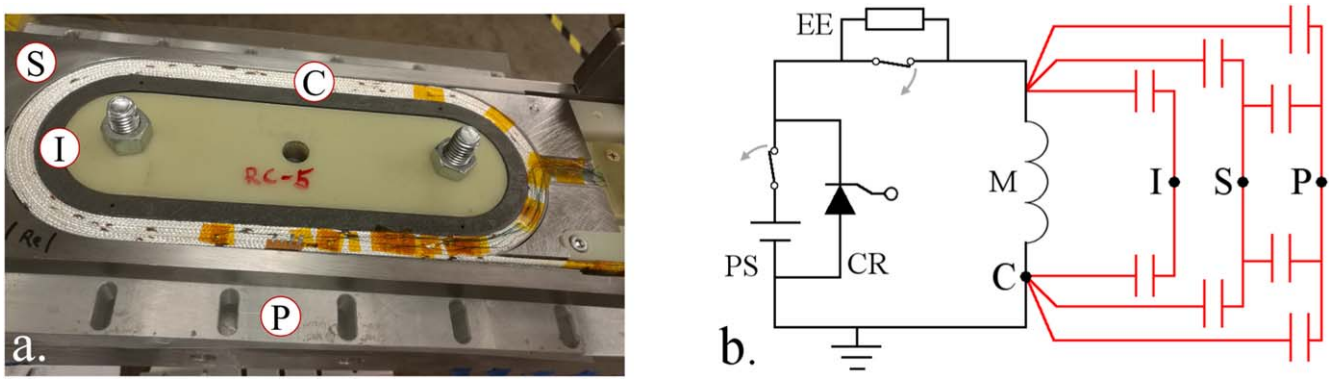


**Figure 2.** One of the $Ag/Bi_2Sr_2CaCu_2O_x$ racetrack magnets on which the stray capacitance quench detection method is applied [31, 32]. (a) Photography showing the coil (C), the pole island (I), the horse-shoe (S), and the plate (P). Half of the plate was removed to show the coil assembly. (b) Simplified electrical scheme of the magnet circuit, composed of a power supply (PS), its crowbar (CR), an energy-extraction system (EE), and the magnet (M). Stray capacitances are indicated in red.

Bi-2212 superconductor and have the same double-pancake geometry [31, 32].

A picture of one of the magnets, showing the elements composing its structure, is shown in figure 2(a). The coil (C) turns are wound around an INCONEL® 600 pole island (I), and are kept in place by a stainless-steel plate (P) and so-called horse-shoes (S) at the ends. The metal parts I, S, and P are insulated from the coil and from each other by an additional 120 $\mu$m layer of kapton. A simplified electrical scheme of the test magnet circuit, including the stray-capacitances between the magnet elements, is shown in figure 2(b).

The main magnet and conductor parameters are summarized in table 1. The conductor is a Rutherford cable composed of 17 strands with a 0.778 mm diameter. Each cable is insulated by a mullite ($2Al_2O_3/SiO_2$) sleeve with an average thickness of 150 $\mu$m.

Key differences between the three tested magnets (RC2, RC3, RC5) are highlighted in table 2. First, their conductor performances are significantly different, following the recent improvement of Bi-2212 critical current [31, 32]. Second, their impregnation schemes are different. In particular, RC2 was impregnated with beeswax to allow an easier coil examination after the test campaign. Lastly, non-negligible ohmic losses were observed in the splices of RC3 and RC5.

The $C$ measurement system is based on a Keysight E4980AL precision LCR meter. In the selected configuration, the instrument continuously applies a 1 V, 300 kHz, AC voltage across two elements to monitor. With these settings, a new value of $C$ is measured every 90 ms. Both, the LCR meter and one magnet current lead grounded to the main earthing line of the test facility. The magnet transport current $I_m$ (A) is mostly unaffected by the applied AC voltage, since the elements I, P, and S are galvanically insulated from the coil.

The six stray capacitances between the four elements C, I, P, and S (see figure 2(b)) were measured in gaseous helium at room temperature, and in a liquid-helium bath with temperature $T_{bath} = 4.2$ K. The values measured for the RC5 magnet are reported in table 3. The most practical stray capacitance signal to monitor is that between P and S, $C_{PS}$ (F). In fact, it was considered prudent to avoid connecting directly the $C$ measurement system to the coil during powering tests. Furthermore, $C_{PS}$ is by far the largest of the available $C$ signals, and thus it is easier to measure a change of its value.

**Table 1.** Main magnet and conductor parameters [31, 32].

| Parameter | Unit | Value |
|---|---|---|
| Superconductor | — | Bi-2212 |
| Stabilizer | — | Ag |
| Insulation | — | $Al_2O_3/SiO_2$ (Mullite) |
| Magnetic transfer function | $T\,A^{-1}$ | $407 \times 10^{-6}$ |
| Number of layers | — | 2 |
| Number of turns per layer | — | 6 |
| Approximate total cable length | m | 8 |
| Strand diameter, after heat treatment | mm | 0.778 |
| Fractions of Ag-0.2wt%Mg, Ag, Bi-2212 | — | 0.25, 0.50, 0.25 |
| Number of strands | — | 17 |
| Cable bare width | mm | 7.80 |
| Cable bare height | mm | 1.46 |
| Filament twist-pitch | — | Untwisted |
| Strand twist-pitch | mm | 55 |
| Insulation thickness | mm | 0.15 |

### *3.1. Capacitance Measurement as a Function of Helium Conditions*

The $C_{PS}$ measured during the RC5 warm-up is plotted in figure 3, as a function of the recorded cryostat temperature. As expected, at the transition between liquid and gaseous phase ($T_{bath} = 4.222$ K), $C_{PS}$ drops due to the helium relative permittivity decrease shown in figure 1. When the magnet is surrounded by gaseous helium, from $T_{bath} = 4.2$ K to room temperature $C_{PS}$ increases with the temperature due to thermal expansion. In fact, in first approximation all sizes of the magnet-structure metallic parts increase by a similar coefficient $\alpha$. Under this simplification, $S$ increases with $\alpha^2$, while $d$ increases with $\alpha$.

**Table 2.** Main differences between the three tested magnets.

| Magnet | Peak current (A) | Impregnation | Splice losses |
|---|---|---|---|
| RC2 [31] | 5782 | Beeswax | Not present |
| RC3 [31] | 6485 | Epoxy NHMFL mix 61 [38, 39] | Present |
| RC5 [32] | 8284 | Epoxy CTD 101k [39–41] | Present |

**Table 3.** Stray capacitances between the elements of rc5 magnet structure, measured in gaseous helium at room temperature and in liquid helium at $T_{bath} = 4.2$ K, in units of pF.

| Room temperature | C | P | S | I | Liquid He | C | P | S | I |
|---|---|---|---|---|---|---|---|---|---|
| C | — | 1329 | 1128 | 260 | C | — | 1145 | 976 | 264 |
| P | — | — | 5696 | 103 | P | — | — | 5233 | 109 |
| S | — | — | — | 92 | S | — | — | — | 101 |

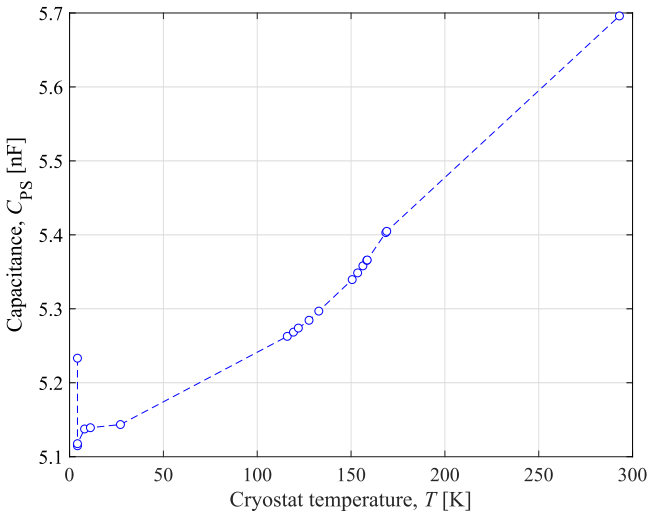


**Figure 3.** Stray capacitance between the plate and the horse-shoe $C_{PS}$, versus cryostat temperature, measured during the warm-up of RC5 magnet.

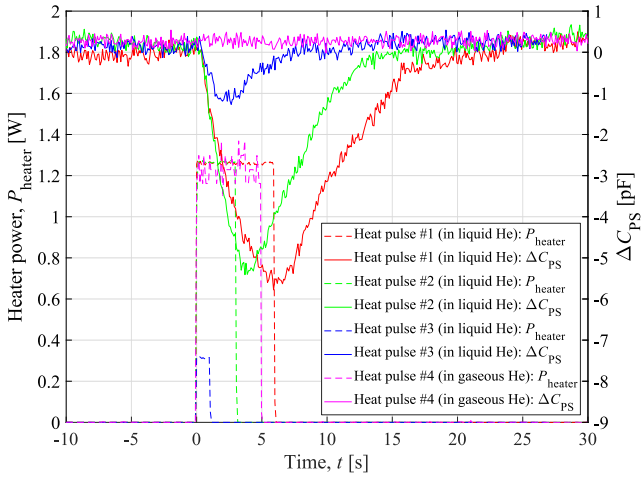


**Figure 4.** RC5 stray capacitance measurement in presence of local heat deposition. Measured $\Delta C_{PS}$ and spot-heater power calculated from the measured heater current ($P_{heater} = R_{heater} I^2_{heater}$, with $R_{heater} = 3.6\ \Omega$), versus time. Comparison between tests conducted in liquid and in gaseous helium for various heat-pulse amplitudes and durations.

The difference between $C_{PS}$ in liquid and gaseous helium at $T_{bath} = 4.2$ K, $|\Delta C_{all\text{-}gas}|$, amounts to about 118 pF, i.e. 2.3%. This amount represents the maximum $C_{PS}$ drop that can be observed during the transient leading to a quench, in the extreme case where all helium impregnating the insulation layers between P and S evaporates. In practical cases, most heat is deposited in a relatively small volume, and hence only part of the impregnating helium can evaporate before a quench occurs.

### *3.2. Capacitance measurement with local heat deposition*

The sensitivity of the $C$ monitoring method was assessed by measuring the capacitance change $\Delta C_{PS}$ in the presence of local heat deposition. A series of tests was conducted, in which square heat pulses of different amplitudes and durations were applied to a 10 mm long heater strip located between the coil outer insulation and the horse-shoe piece.

The experimental results of four such tests are shown in figure 4. An appreciable $\Delta C_{PS}$ was measured for heat deposition as low as 0.3 J during heat-pulse tests performed in liquid helium at $T_{bath} = 4.2$ K. $C_{PS}$ returned to its original value when the evaporated liquid helium re-impregnated fully the magnet insulation layers. This process took several tens of seconds.

Interestingly, no $\Delta C_{PS}$ was observed during the test conducted in gaseous helium. This is expected, since the helium relative permittivity change is minimal in the gaseous phase, as observed in figure 1.

## 4. Calibration of the stray-capacitance monitoring system

The three Bi-2212 magnets were tested individually in liquid helium. Their operational quench detection was based on a conventional voltage-tap system, with a voltage threshold of 20 mV (for RC3) or 100 mV (for RC2 and RC5). Simultaneously, the

**Table 4.** Qualitative description of thermal regimes in hts coils.

| Regimes | Conductor temperature | Current | Ohmic loss |
|---|---|---|---|
| No transport current | $T = T_{bath}$ | 0 | 0 |
| Superconducting (SC) | $T < T_{cs}$ | 100% in SC | 0 |
| Current sharing | $T_{cs} < T < T_c$ | Shared | $P_{ohm} < P_{cooling}$ |
| Thermal runaway | $T > T_c$ | Shared | $P_{ohm} > P_{cooling}$ |

capacitance $C_{PS}$ was monitored to gather additional information about the magnet behavior.

### 4.1. Current sharing regime in Ag/Bi-2212 coil

In order to better understand the $C$ changes observed during the experiments, the current-sharing regime in the tested coils is briefly described. The four regimes qualitatively characterizing the coil thermal behavior are listed in table 4. When no current flows in the coil windings, the conductor temperature $T$ (K) is at the equilibrium with $T_{bath}$. When $I_m > 0$, the conductor remains fully superconducting if $T$ is lower than the current-sharing temperature $T_{cs}$ (K). If $T > T_{cs}$, part of the current flows through the superconductor (SC), and part through the Ag matrix. Hence, local ohmic loss arises. The magnet remains in this current-sharing regime without quenching if $T$ is lower than the critical temperature $T_c$ (K) and if locally the ohmic loss is lower than the cooling of the cryogenic fluid, i.e. $P_{ohm} < P_{cooling}$. Due to the high stability of the Ag/Bi-2212 conductor, the magnet can be operated in the current-sharing regime for long periods of time, even in the presence of relatively high ohmic loss [31]. When $P_{ohm} > P_{cooling}$, a thermal runaway occurs, which leads to a fast increase of $T$ and to a quench.

### 4.2. Stray-capacitance monitoring during powering tests

In order to investigate the coil behavior at different current levels, the current of magnet RC3 was set to increase following the staircase pattern shown in figure 5. The current was brought at different levels between 3.04 and 6.25 kA, and held steady for 120 s at each level. The same ramp-rate of $dI_m/dt = 25\ A\ s^{-1}$ was used for all the ramps.

The measured voltage across the coil $\Delta U$ (V) during the power test is plotted in figure 5. Its signal was digitally filtered using a multi-band notch filter to reduce the noise introduced by the power supply. During each current ramp, a positive inductive voltage develops across the coil, i.e. $\Delta U > 0$. During the plateaux, the inductive voltage is not present, and hence if the coil was fully superconducting $\Delta U$ would be nil. However, for $I_m$ higher than about 5 kA, a non-zero $\Delta U$ develops. This indicates that around that current the coil enters the current-sharing transition described in section 4.1, and hence a resistive voltage arises across it. The amplitude of the observed resistive voltage is in the order of tens to hundreds of $\mu$V.

Furthermore, the measured voltage across the coil and its two splices $\Delta U + \Delta U_{splices}$ (V) is plotted in figure 5. A non-zero $\Delta U_{splices}$ can be observed at current levels higher than about 3 kA. This indicates that a certain ohmic loss is generated in the splices even before the coil enters the current-sharing regime.

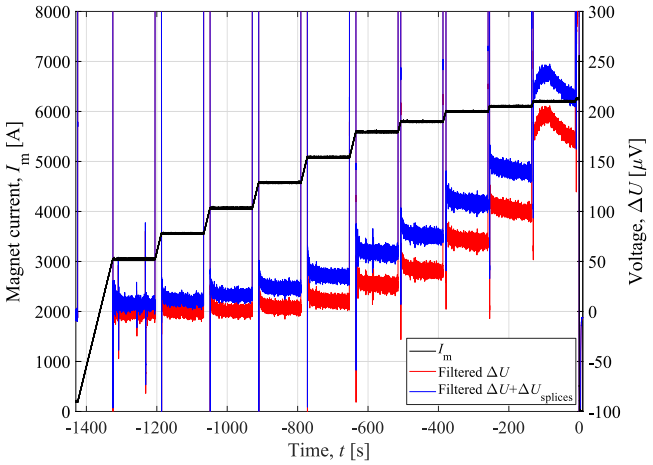


**Figure 5.** RC3 powering test. Measured magnet current, voltage across the coil, and voltage across coil and its splices, versus time. Voltage signals were digitally filtered to reduce noise.

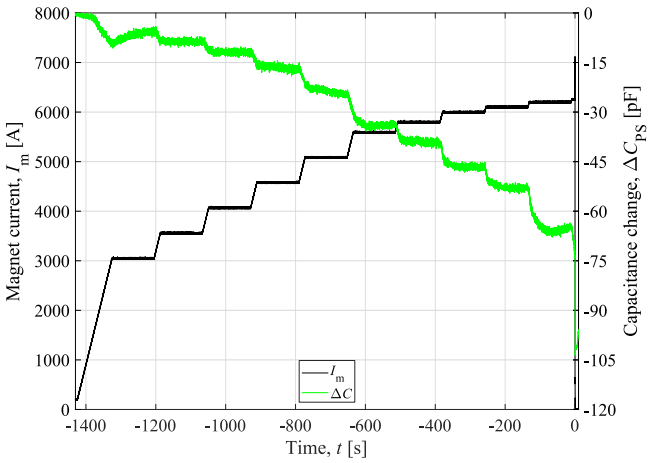


**Figure 6.** RC3 powering test. Measured magnet current and stray capacitance $\Delta C_{PS}$, versus time.

The stray capacitance $\Delta C_{PS}$ was monitored during the same powering test, and is plotted in figure 6. Whenever heat is locally generated in the coil, a certain amount of helium impregnating the insulation layers evaporates, and a reduction of $\Delta C_{PS}$ is observed. In this transient, heat is generated mainly due to three contributions: coupling loss, ohmic loss in the conductor, and ohmic loss in the splices. Coupling loss occurs during the current ramps due to the magnetic-field change imposed by the transport current variation [42, 43].

For example, the drop of $\Delta C_{PS}$ during the first ramp to 3 kA, while no resistive voltage was observed, is due to coupling loss. Note that when the current stops increasing and the coupling loss vanishes, $\Delta C_{PS}$ drifts back towards its initial value. Ohmic losses in the conductor and in the splices cause local heat deposition. A balance is reached between ohmic loss and helium cooling a few seconds after $I_m$ reaches each new current level. During this condition the temperature distribution in the conductor, and hence the amount of evaporated helium, remain unvaried. Thus, a relatively stable value of $\Delta C_{PS}$ can be observed at each current level. A system monitoring the $C$ change is sensitive to all heat depositions, but does not provide information about their sources nor locations.

A thermal runaway occurred about 9 s after reaching the last plateau at $I_m = 6.25$ kA. $\Delta U$ reached the 20 mV voltage threshold in a few tens of milliseconds after the thermal runaway started due to the fast resistive voltage built-up (see figure 5). Simultaneously, a significant drop is visible in the $\Delta C_{PS}$ signal, which reaches the value $\Delta C_{all\text{-}gas}$, corresponding to the condition at which all helium impregnating the insulation layers is evaporated. Given the poor time resolution of the $C$ monitoring system, which stores a new data point every 90 ms, it is not clear whether the $\Delta C_{PS}$ drop occurs during the thermal runaway, i.e. just before $t = 0$, or after the quench is detected by the voltage-tap system and a fast energy-extraction is triggered. Coupling loss developed during the fast discharge could easily explain the observed $\Delta C_{PS}$ drop. Future tests with faster acquisition frequency will allow determining more precisely the moment when the largest $\Delta C_{PS}$ drop occurs.

Similar powering tests were performed on the RC2 and RC5 magnets as well. The measured $\Delta U$, $\Delta U + \Delta U_{splices}$, and $\Delta C_{PS}$ at each current level are plotted in figure 7. As indicated in table 2, the three coils are made of superconductors with different performances, and can reach significantly different peak currents. Hence, the current-sharing regime occurs at different current levels.

At higher $I_m$, a larger fraction of the transport current flows through the Ag matrix, and hence higher ohmic loss is locally deposited. As a result, the conductor resistance per unit length and the resistive voltage increase. For each coil, measured voltages and capacitance changes generally exhibit a similar dependence on $I_m$. This occurs because at higher $I_m$ the additional heat evaporates a larger amount of the helium impregnating the insulation layers, and the gaseous helium has lower $\epsilon_r$.

Note that the $\Delta U$ voltages presented here are measured across the entire length of the conductor, which is about 8 m long. Therefore, they are not suitable for deriving the superconductor $n$-values. The $n$-value of the RC5 superconductor derived from the highest magnetic-field turn, which is about 14 cm long, is 22 [32].

For each coil, the highest current plotted in figure 7 corresponds to the highest current level at which the coil could be operated for 120 s without the occurrence of a thermal runaway. The maximum $C$ change, observed at the highest $I_m$, is defined as $\Delta C_{max,steady}$ (F). The values of

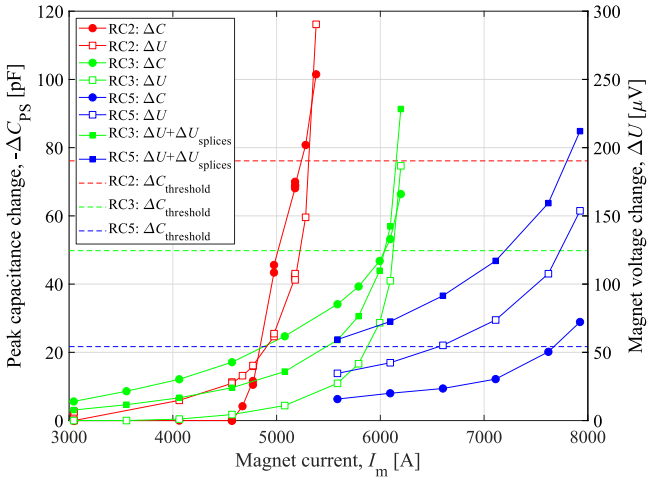


**Figure 7.** Comparison between measured magnet voltage change across the coil, including the voltage drop across the splices or not, and P–S capacitance change, versus current level. Data obtained from three different Bi-2212 coils in liquid helium at $T_{bath} = 4.2$ K, during 120 s long plateaux at constant current. $\Delta C$ thresholds selected for each coil (see table 5) are indicated with dashed lines. Note that the $\Delta U$ voltages presented here are measured across the entire length of the conductor, which is about 8 m, and therefore are not suitable for deriving the superconductor $n$-values. The $n$-value of the RC5 superconductor derived from the highest magnetic-field turn, which is about 14 cm long, is 22 [32].

**Table 5.** Characteristic stray capacitance differences of the three tested magnets.

| Magnet | $\lvert\Delta C_{all\text{-}gas}\rvert$ [pF] | $\lvert\Delta C_{max,steady}\rvert$ (pF) | $\lvert\Delta C_{threshold}\rvert$ (pF) | Noise of $\lvert\Delta C_{PS}\rvert$ (pF) |
|---|---|---|---|---|
| RC2 | 147 | 101 | 76 | <1 |
| RC3 | 111 | 66 | 50 | <0.3 |
| RC5 | 124 | 29 | 22 | <0.05 |

$\Delta C_{max,steady}$ for the three coils are reported in table 5, and compared to the respective $\Delta C_{all\text{-}gas}$ values. RC2 coil's values are higher than for the other coils. This could be explained by the different impregnation scheme: for RC2 beeswax was used, whereas for RC3 and RC5 epoxy was used. Since beeswax is more porous than epoxy, it is expected that a larger amount of helium can penetrate a beeswax-based impregnation, and hence allow for a larger overall $C$ change when evaporation occurs.

The characteristic noise observed on the $\Delta C_{PS}$ signal varies considerably between coils. The ratios between the noise and the characteristic $\lvert\Delta C_{max,steady}\rvert$ are about 1.0%, 0.5%, and 0.2% for the RC2, RC3, and RC5 coils, respectively. Since beeswax is much softer than epoxy, it is expected that higher noise occurs when monitoring the RC2 coil. In fact, in this coil the conductor is not as well maintained in place and local coil movements can easily lead to $C$ measurement noise. The difference between the noise levels in RC3 and RC5 is presently not fully understood. A possible explanation for this result is the use of different epoxies in the impregnation scheme, as shown in table 2.

The relatively high noise observed during RC2 tests does not allow a reliable detection of very low heat depositions. This is the reason why $\Delta C_{PS}$ shows an appreciable change only above $I_m = 4.6$ kA, while $\Delta U$ is above zero already at 4 kA.

Monitoring $C$ allows detecting any heat deposition that results in the evaporation of cryogenic fluid impregnating the insulation layers. In the present system, this includes heat deposited in the coil splices. For example, a measurable $\Delta C_{PS}$ is observed for RC3 at $I_m$ as low as 3 kA. The presence of heating in the splices is confirmed by the measured $\Delta U + \Delta U_{splices}$. However, no heat is generated in the RC3 superconductor for $I_m < 4.5$ kA, and hence $\Delta U \approx 0$.

The tests conducted on the three coils confirm that the proposed $C$ monitoring technique can be used as a means to detect heat deposited in a coil and its splices during the current-sharing regime.

### *4.3. Selection of stray-capacitance detection thresholds*

In order to implement the method in a quench detection system, a threshold $\Delta C_{threshold}$ (F) must be selected for the monitored $\Delta C$. Different peak stray-capacitance changes are achieved in the three different coils due to their different characteristics. Thus, a specific threshold need to be set for each individual coil. Here, we propose to select thresholds equal to 75% of $|\Delta C_{max,steady}|$. The three thresholds, listed in table 5 and indicated in figure 7, are 75–440 times higher than their respective noise levels. Thus, they provide a conservative margin with respect to the heat deposition that causes a thermal runaway, while remaining much higher than the noise.

In future implementations of the stray-capacitance detection method, it is envisaged that dedicated capacitive sensors of well-known dimensions and characteristics will be installed on the coil to protect. In that case, the detection threshold will be defined during the design phase, instead of deriving it empirically after powering tests are performed.

The measured $\Delta C_{PS}$ at various current levels are plotted in figure 8 as a function of the calculated power deposited in the coil, together with the three selected $\Delta C_{threshold}$. The implemented $\Delta C$ monitoring system is sensitive to a deposited heat as low as 25 mW. In comparison, thermal runaway did not start in the coils even in the presence of 1.4–1.7 W deposited power. The chosen $\Delta C_{threshold}$ result in a detection when the deposited heat is about 1 W.

## 5. Quench detection with the stray-capacitance monitoring system

The proposed $C$ monitoring system is used to detect thermal runaways occurring in the three tested Bi-2212 magnets in liquid helium at $T_{bath} = 4.2$ K. Various examples of quench detection under different operating scenarios are presented and discussed. The quench tests are of two types: thermal runaways due to ohmic loss in the current-sharing regime, and heater-induced quenches.

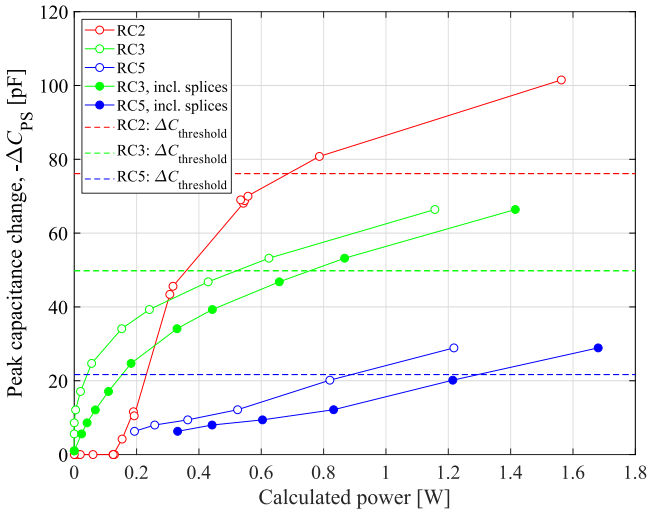


**Figure 8.** Measured P–S capacitance change versus power deposited in the coil, calculated from measured $\Delta U I_m$ and $(\Delta U + \Delta U_{splices})$ $I_m$. Data obtained from three different Bi-2212 coils in liquid helium at $T_{bath} = 4.2$ K, during 120 s long plateaux at constant current. $\Delta C$ thresholds selected for each coil (see table 5) are indicated with dashed lines.

### *5.1. Detection of thermal runaways*

When no current flows in a magnet, the stray capacitances return to their unperturbed value. This process usually takes several tens of seconds. The transport current and the P–S stray-capacitance change with respect to its unperturbed value, measured during thermal runaways that occurred in the RC2 coil, are shown in figure 9. In each test, $I_m$ was ramped up to an intermediate level of 5.1 kA, held for a few seconds, then ramped to a higher level, and finally held until thermal runaway occurred. During the last step, the current was held for about 20.1, 8.1, and 3.2 s at 5.43, 5.48, and 5.58 kA before a quench occurred, respectively [30]. The higher the current level, the higher the ohmic loss, and the faster a runaway occurred.

When approaching the current level at which thermal runaway occurs, $\Delta C_{PS}$ changes significantly. It can be easily verified that $\Delta C_{PS}$ is not proportional to $I_m$, nor its time derivative. Hence, it is highly unlikely that the observed $C$ change is an artefact due to ground loops or inductive pick-ups. Furthermore, $\Delta C_{PS}$ is not proportional to $I_m^2$, which rules out electro-mechanical forces as the main cause of the observed $C$ change.

$\Delta C_{PS}$ reached its threshold 18, 9, and 3 s before the thermal runaway actually occurred, respectively. During the same transients, the measured $\Delta U$ remained below 1 mV until about 2 s before the runaway, and increased from about 10 mV to the 100 mV threshold during the last 200 ms before the thermal runaway. In all transients analyzed in the rest of the paper, $t = 0$ corresponds to the time at which the voltage-tap based quench detection system was triggered.

For the same current level, $\Delta C_{PS}$ reached lower values than those measured during 120 s long current plateaux in the range of 5.1–5.4 kA, previously shown in figure 7. This is explained by the fact that during these faster transients the

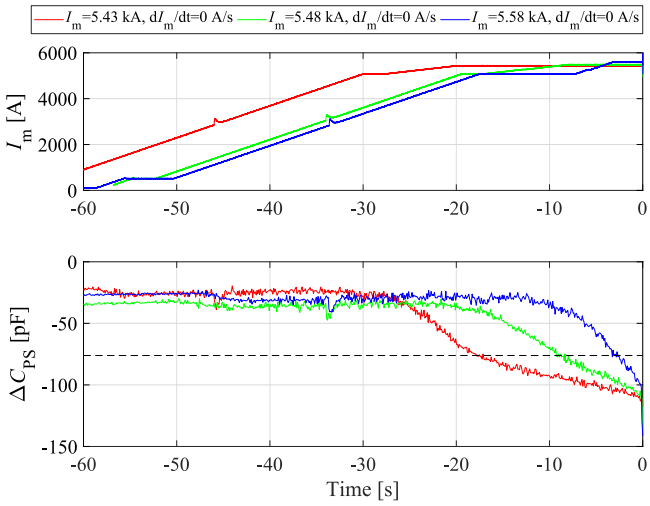


**Figure 9.** Thermal runaway detection in RC2 coil in liquid helium at $T_{bath} = 4.2$ K, using the proposed stray-capacitance monitoring system. Measured transport current (upper plot) and P–S capacitance change (lower plot) versus time. The proposed detection threshold $\Delta C_{threshold}$ is indicated with a black dashed line. Quenches occurred while holding $I_m$ at different current levels.

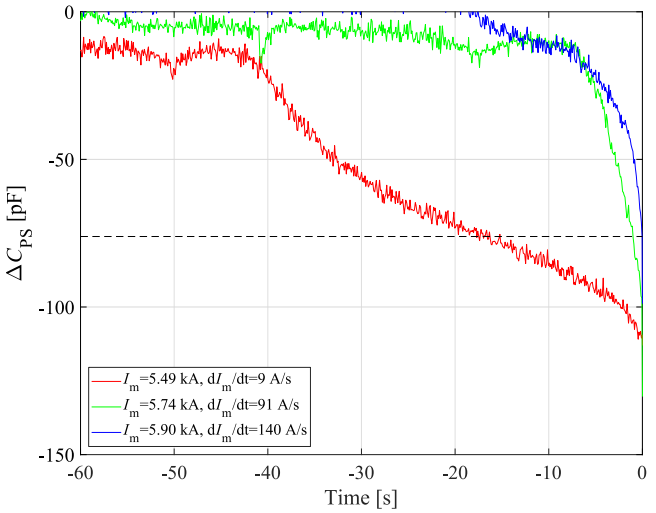


**Figure 10.** Thermal runaway detection in RC2 coil in liquid helium at $T_{bath} = 4.2$ K, using the proposed stray-capacitance monitoring system. Measured P–S capacitance change versus time. Quenches occurred while ramping $I_m$ with different current ramp-rates. The proposed detection threshold $\Delta C_{threshold}$ is indicated with a dashed line.

magnet does not dwell at each current level, and hence significantly less ohmic loss in current-sharing regime is deposited. As a result, less helium is boiled off, and lower $|\Delta C_{PS}|$ is reached.

This result leads to the observation that $\Delta C_{PS}$ does not only depend on the instantaneous heat (power) dissipated in the coil, but also on the total heat generated and evacuated by helium during the transient (energy). The same conclusion is reached when comparing thermal runaways occurred during current ramp-ups with different ramp-rates. $I_m$ and $\Delta C_{PS}$ measured during three such transients are shown in figure 10. When ramping up with higher $dI_m/dt$, less ohmic heat is generated to reach the same current level. In fact, in this condition the magnet spends a shorter time at high current, when ohmic loss in current sharing regime is high. Thus, lower $|\Delta C_{PS}|$ is reached at the moment of the thermal runaway. The $\Delta C_{threshold}$ was reached 17 s, 1 s, and 30 ms before the thermal runaway for a $dI_m/dt$ of 9, 91, and 140 A s$^{-1}$, respectively. The observation that lower heat is deposited in the coil during higher $dI_m/dt$ ramp-ups is also sustained by the fact that higher peak current was reached for higher $dI_m/dt$ [31].

Similar tests were conducted on the RC3 magnet, and qualitatively the same results were obtained. $I_m$ and $\Delta C_{PS}$ measured during five transients leading to thermal runaways are shown in figure 11. During two of these transients, $I_m$ was ramped up until a quench occurred. The $\Delta C_{threshold}$ was reached 6 and 0.5 s before the thermal runaway for a $dI_m/dt$ of 25 and 128 A s$^{-1}$, respectively. As in the case of RC2, $\Delta C$-based quench detection proved more challenging for higher ramp-rates.

In the other three transients, $I_m$ was held for several tens of seconds at a fixed level, and subsequently ramped with $dI_m/dt = 4$ A s$^{-1}$ until quench. The selected current levels

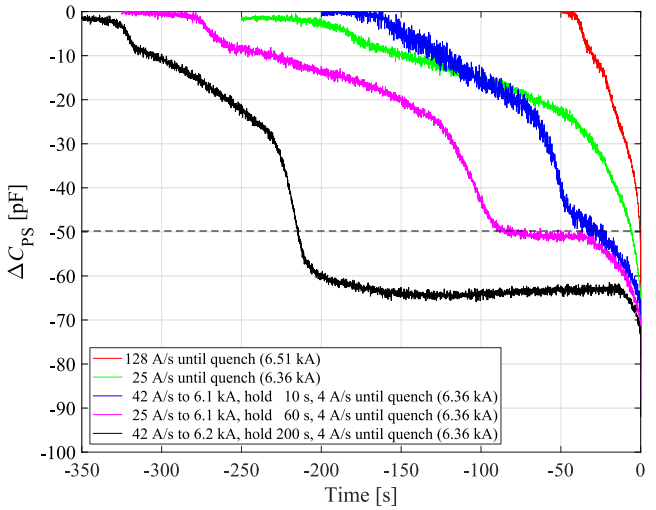


**Figure 11.** Thermal runaway detection in RC3 coil in liquid helium at $T_{bath} = 4.2$ K, using the proposed stray-capacitance monitoring system. Measured P–S capacitance change versus time. The proposed detection threshold $\Delta C_{threshold}$ is indicated with a black dashed line. Quenches occurred while submitting $I_m$ to different transients, which are described in the legend.

were very close to the highest current at which RC3 can be operated without leading to a thermal runaway, i.e. 6.2 kA. As previously shown in figure 7, the magnet can be operated in steady state in the range 5.5 kA $< I_m <$ 6.2 kA, but a significant resistive voltage develops across it. As a result, $\Delta C_{PS}$ changes considerably. The magnet can reach and maintain a steady $\Delta C_{PS}$ value if the local ohmic loss is balanced by the helium cooling. However, if the magnet is close to the level at which thermal runaway occurs $|\Delta C_{PS}| > \Delta C_{threshold}$. Thus, the selected threshold would prevent operating RC3 during these three transients, as can be

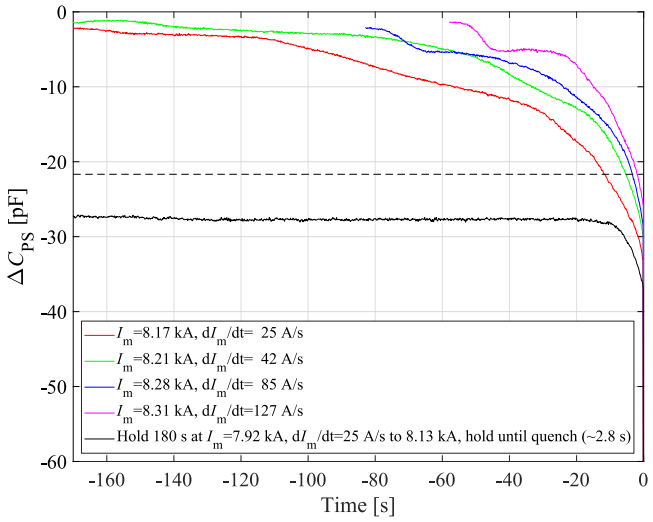


**Figure 12.** Thermal runaway detection in RC5 coil in liquid helium at $T_{bath} = 4.2$ K, using the proposed stray-capacitance monitoring system. Measured P–S capacitance change versus time. The proposed detection threshold $\Delta C_{threshold}$ is indicated with a black dashed line. Quenches occurred while ramping $I_m$ with different current ramp-rates.

observed in figure 11. $\Delta C_{threshold}$ was reached several tens of seconds before the thermal runaway started.

Even earlier detection was achieved during similar tests conducted on the RC5 magnet. The experimental results from five thermal runaways are shown in figure 12. The much lower observed noise allows for a noticeably clearer detection of local heating. The selected $\Delta C_{threshold}$ was reached 2 and 12 s before thermal runaway during ramp-ups with $dI_m/dt$ of 25 and 127 A $s^{-1}$, respectively.

During a different test, the magnet current was held for several minutes at a level of almost 8 kA. As observed in figure 7, in this condition the coil is very close to a thermal runway. The chosen $\Delta C_{threshold}$ would have prevented operating the magnet in this regime, since $|\Delta C_{PS}| > \Delta C_{threshold}$. During this transient, more than 1.5 W of ohmic power was constantly deposited in the coil and its splices.

### *5.2. Detection of induced quenches*

Additional tests were performed, during which the magnet current was held at a certain level and square heat pulses were applied to a 10 mm long heater strip located between the coil outer insulation and the horse-shoe piece. This allowed investigating the sensitivity of the proposed detection methods to localized heat deposition.

The results of such tests performed on the RC3 magnet are shown in figure 13(a). Square, 1 s long heat pulses of amplitudes in the range of 0.6–22.1 W were introduced until a quench was induced at $t = 0$. $\Delta C_{PS}$ visibly changed after each heat pulse was triggered. When local heat was deposited, part of the helium impregnating the insulation layers evaporated, which resulted in a sudden reduction of $\Delta C_{threshold}$ of several pF, or tens of pF. After each heat pulse, $\Delta C_{PS}$ changed

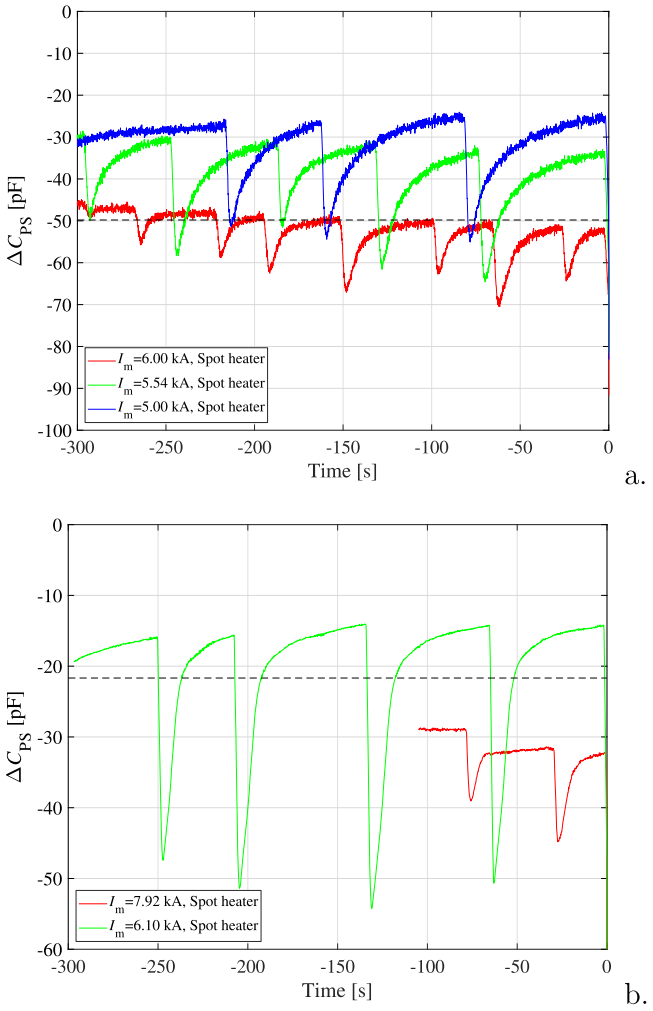


**Figure 13.** Detection of spot-heater induced quenches in two coils in liquid helium at $T_{bath} = 4.2$ K, using the proposed stray-capacitance monitoring system. Measured P–S capacitance change versus time. Heat pulses of different amplitude and duration were introduced until quench occurred, while $I_m$ was held steady. The proposed detection thresholds $\Delta C_{threshold}$ are indicated with dashed lines. (a) RC3 coil. (b) RC5 coil.

back towards the value it had before local heating occurred. This process took several tens of seconds.

At each current level, only the very last heat pulse deposited sufficient heat to start a thermal runaway. However, $\Delta C_{threshold}$ was reached after each heat pulse. Depending on the application, this high sensitivity to local heat deposition might be desirable or not. On the one hand, it allows early detection of any local heating. On the other hand, it can result in spurious detection if heating occurs without leading to a thermal runaway.

Similar spot-heater tests were performed on the RC5 magnet. The $\Delta C_{PS}$ measured during the transients following 1 s long heat pulses of amplitudes in the range of 2.5–22.5 W are shown in figure 13(b). At $I_m = 6.10$ kA, all heat pulses caused a reduction of $\Delta C_{PS}$ that exceeded $\Delta C_{threshold}$. At $I_m = 7.92$ kA , $|\Delta C_{PS}| > \Delta C_{threshold}$ already before introducing any heat pulse.

The results reported in this section indicate that the proposed stray-capacitance monitoring system is sensitive to localized heat depositions, which can potentially lead to a quench.

## 6. Discussion

The proposed method based on stray-capacitance monitoring was proven to be sufficiently sensitive to effectively detect local heating of the conductor before a quench. The primary mechanism leading to $C$ change was identified as the variation of electrical permittivity of the cryogenic fluid impregnating insulation layers between coil parts. The highest electrical permittivity change occurs when the fluid is transferred from the liquid to the gaseous phase. Thus, in the case of magnets operated in liquid helium, the method is most sensitive to heating increasing the local temperature above 4.222 K. Given the high temperature margin with respect to quench in HTS magnets, it is expected that a significant $C$ change will occur well before the quench occurs.

The early detection of local heating carries advantages and disadvantages. On the one hand, it offers high sensitivity to heat deposited anywhere in the coil and its splices, which can prevent high continuous cryogenic loss during operation, and ultimately a thermal runaway. Moreover, the monitored signal is independent of the type of heating source. On the other hand, if the local heat deposition is insufficient to start a quench, but sufficient to evaporate part of the helium impregnating the insulation layers, spurious quench detection can be triggered. The observed $C$ change is related to the amount of boiled-off helium, and not directly to the likelihood of a quench.

This monitoring technique is well-suited to be implemented together with the conventional voltage-tap based method. In fact, it relies on a completely different detection mechanism and can offer complementary information about the quench development.

Furthermore, a stray-capacitance detection system can be implemented unobtrusively without any direct electrical connection to the coil to monitor. In the presented configuration, the capacitance between existing magnet-structure elements has been monitored. In future applications, dedicated capacitive detection sensors are envisaged, whose implementation will offer considerable advantages. First, their dimensions and the amount of impregnating helium will be known with greater precision, which in turn will allow a more quantitative definition of the detection threshold. Second, their location can be optimized to improve sensitivity of the method to heating in specific coil positions. Third, they can be constrained more securely, so that mechanical movements and the noise associated with them are reduced.

In the first analysis, it appears the method can be successfully scaled to longer magnets. In fact, the amplitude of the $\Delta C$ signal during a quench is affected by the local heating, which is independent of the magnet length. However, the absolute value of $C$ increases for longer magnets, and as a consequence the background noise could increase as well.

The main limitation of the proposed method is the fact that it relies on phase change of the cryogenic fluid. Thus, it cannot be applied for detecting a quench occurring in a magnet operated in gas.

Another shortcoming is the electro-magnetic coupling between the detection system and the magnet electrical circuit, which brings two potential drawbacks. First, electrical perturbations in the magnet circuit can cause $C$ change even in absence of heating. Second, the applied voltage used for monitoring $C$ might introduce a high-frequency noise on the magnet voltage. Both issues will be addressed in future work.

## 7. Conclusion

A new quench detection method was developed, which utilizes the stray-capacitance change between electrically-insulated magnet elements as an indication of local heat deposition in the conductor. The main mechanism causing the capacitance variation is the change of electrical permittivity of the cryogenic fluid impregnating the insulation layers. A considerable permittivity change occurs when the fluid is transferred from the liquid to the gaseous phase. When heat is locally deposited in the conductor, part of the fluid impregnating the insulation layers evaporates. Thus, stray-capacitance variation occurs after heating from any source that cause local helium boil-off. The proposed technique is particularly promising for high-temperature superconductor magnets operated in cryogenic liquid. The critical temperature of high-temperature superconductors is well above helium boiling temperature, and thus significant stray-capacitance change is expected before the quench even starts.

The technique was successfully tested on three small-scale $Ag/Bi_2Sr_2CaCu_2O_x$ magnets manufactured at the Lawrence Berkeley National Laboratory. These coils are characterized by a fairly broad current-sharing regime. Hence, they can be operated in liquid helium for tens of seconds at a current level at which ohmic loss constantly occurs. Stray-capacitance change at different magnet current levels was observed, indicating local heat deposition. The presence of a small resistive voltage developed across the coils was confirmed by independent voltage-tap measurements performed during the same tests.

Significant stray-capacitance changes were observed during the transients leading to thermal runaways. For the three coils, capacitance changes higher than the selected detection thresholds occurred seconds, or even tens of seconds, before the quench occurred. Early detection was achieved more easily for ramp-ups with lower ramp-rate, during which more heat was deposited in the coil.

Sensitivity to localized heat deposition was successfully demonstrated by introducing 1 s heat pulses with a 10 mm long spot heater. Stray-capacitance changes above the detection threshold were observed after each heat pulse. An appreciable capacitance change was measured for heat deposition as low as 0.3 J.

The proposed stray-capacitance monitoring method appears a good solution for quench detection in high-temperature

superconductor based coils and conductors immersed in cryogenic liquid due to its early heating detection and unobtrusiveness. It does not rely on any direct electrical connection to the coil to protect. It is based on a different physical principle with respect to the conventional voltage-tap quench detection system. Thus, it can be implemented along with voltage taps to provide complementary information about the quench behavior and the coil stability.

A few shortcomings were identified during the first tests of the proposed system. The monitored capacitance can be temporarily perturbed by electro-magnetic transients occurring in the magnet circuit, and drift in time due to variation of the cryogenic conditions. Future developments are considered to address these issues, reduce the noise level, and define more precise detection thresholds. In particular, the implementation of dedicated capacitive sensors of known, controlled dimensions and characteristics, as opposed to utilizing the existing magnet-structure elements, might be particularly beneficial.

## Acknowledgments

The authors wish to thank H Higley, J Taylor, and M Turqueti (LBNL) for their help during the coil manufacturing and testing.

Work at LBNL was supported by the Director, Office of Science of the US Department of Energy (DOE) under Contract No. DE-AC02-05CH11231 and also by a US DOE early career award.

K Zhang acknowledges support from the China Scholarship Council.

D Davis acknowledges support from the US DOE Office of Science Graduate Student Research Program.

## ORCID iDs

E Ravaioli https://orcid.org/0000-0002-7651-5313
T Shen https://orcid.org/0000-0003-1581-320X

## References

[1] Pfotenhauer J M, Kessler F and Hilal M A 1993 Voltage detection and magnet protection *IEEE Trans. Appl. Supercond.* **3** 273–6

[2] Shen T, Ye L and Li P 2016 Feasible voltage-tap based quench detection in a Ag/Bi-2212 coil enabled by fast 3D normal zone propagation *Supercond. Sci. Technol.* **29** 08LT01

[3] Bellis R H and Iwasa Y 1994 Quench propagation in high tc superconductors *Cryogenics* **34** 129–44

[4] Trillaud F, Palanki H, Trociewitz U P, Thompson S H, Weijers H W and Schwartz J 2003 Normal zone propagation experiments on HTS composite conductors *Cryogenics* **43** 271–9

[5] Wang X, Caruso A R, Breschi M, Zhang G, Trociewitz U P, Weijers H W and Schwartz J 2005 Normal zone initiation and propagation in Y–Ba–Cu–O coated conductors with Cu stabilizer *IEEE Trans. Appl. Supercond.* **15** 2586–9

[6] Song S, Lee J, Lee W S, Jin H, Lee J, Hwang Y J and Ko T K 2015 Quench detection method for HTS coils using electromagnetically coupled coils *IEEE Trans. Appl. Supercond.* **25** 1–4

[7] Kim Y O *et al* 2016 Development and experimental evaluation of a prototype of the tf secondary quench detection system for kstar device *IEEE Trans. Plasma Sci.* **44** 1758–62

[8] Ninomiya A, Sakaniwa K, Kado H, Ishigohka T and Higo Y 1989 Quench detection of superconducting magnets using ultrasonic wave *IEEE Trans. Magn.* **25** 1520–3

[9] Kim H M, Park K B, Lee B W, Oh I S, Sim J W, Hyun O B, Iwasa Y and Lee H G 2007 A stability verification technique using acoustic emission for an HTS monofilar component for a superconducting fault current limiter *Supercond. Sci. Technol.* **20** 506

[10] Kim K J, Song J B, Kim J H, Lee J H, Kim H M, Kim W S, Na J B, Ko T K and Lee H G 2010 Detection of AE signals from a HTS tape during quenching in a solid cryogen-cooling system *Proc. 22nd Int. Symp. on Superconductivity (ISS 2009); Physica* C **470** 1883–6

[11] Yoneda M, Nanato N, Aoki D, Kato T and Murase S 2011 Quench detection/protection of an HTS coil by AE signals *23rd Int. Symp. on Superconductivity; Physica* C **471** 1432–5

[12] Marchevsky M, Sabbi G, Bajas H and Gourlay S 2015 Acoustic emission during quench training of superconducting accelerator magnets *Cryogenics* **69** 50–7

[13] Marchevsky M and Gourlay S A 2017 Acoustic thermometry for detecting quenches in superconducting coils and conductor stacks *Appl. Phys. Lett.* **110** 012601

[14] Leroy D, Krzywinski J, Remondino V, Walckiers L and Wolf R 1993 Quench observation in LHC superconducting one meter long dipole models by field perturbation measurements *IEEE Trans. Appl. Supercond.* **3** 781–4

[15] Ogitsu T, Devred A, Kim K, Krzywinski J, Radusewicz P, Schermer R I, Kobayashi T, Tsuchiya K, Muratore J and Wanderer P 1994 Quench antenna for superconducting particle accelerator magnets *IEEE Trans. Magn.* **30** 2273–6

[16] Ogitsu T, Terashima A, Tsuchiya K, Ganetis G, Muratore J and Wanderer P 1996 Quench observation using quench antennas on RHIC IR quadrupole magnets *IEEE Trans. Magn.* **32** 3098–101

[17] Jongeleen S, Leroy D, Siemko A and Wolf R 1997 Quench localization and current redistribution after quench in superconducting dipole magnets wound with Rutherford-type cables *IEEE Trans. Appl. Supercond.* **7** 179–82

[18] Sasaki K, Ogitsu T, Ohuchi N and Tsuchiya K 1998 Study of quench propagation with quench antennas *Nucl. Instrum. Methods Phys. Res.* A **416** 9–17

[19] Marchevsky M, DiMarco J, Felice H, Hafalia A R, Joseph J, Lizarazo J, Wang X and Sabbi G 2013 Magnetic detection of quenches in high-field accelerator magnets *IEEE Trans. Appl. Supercond.* **23** 9001005

[20] Marchevsky M, Hafalia A R, Cheng D, Prestemon S, Sabbi G, Bajas H and Chlachidze G 2015 Axial-field magnetic quench antenna for the superconducting accelerator magnets *IEEE Trans. Appl. Supercond.* **25** 1–5

[21] van Oort J M, Scanlan R M and ten Kate H H J 1995 A fiber-optic strain measurement and quench localization system for use in superconducting accelerator dipole magnets *IEEE Trans. Appl. Supercond.* **5** 882–5

[22] Soller B J, Gifford D K, Wolfe M S, Froggatt M E, Yu M H and Wysocki P F 2006 Measurement of localized heating in fiber optic components with millimeter spatial resolution *2006 Optical Fiber Communication Conf. and the National Fiber Optic Engineers Conf.* p 3

[23] Chan W K, Flanagan G and Schwartz J 2013 Spatial and temporal resolution requirements for quench detection in (RE)$Ba_2Cu_3O_x$ magnets using Rayleigh-scattering-based

fiber optic distributed sensing *Supercond. Sci. Technol.* **26** 105015
[24] Scurti F, Ishmael S, Flanagan G and Schwartz J 2016 Quench detection for high temperature superconductor magnets: a novel technique based on Rayleigh-backscattering interrogated optical fibers *Supercond. Sci. Technol.* **29** 03LT01
[25] Scurti F and Schwartz J 2017 Optical fiber distributed sensing for high temperature superconductor magnets *2017 25th Optical Fiber Sensors Conf. (OFS)* pp 1–4
[26] Scurti F, Sathyamurthy S, Rupich M and Schwartz J 2017 Self-monitoring 'SMART' (Re)$Ba_2Cu_3O_{7-x}$ conductor via integrated optical fibers *Supercond. Sci. Technol.* **30** 114002
[27] Scurti F, McGarrahan J and Schwartz J 2017 Effects of metallic coatings on the thermal sensitivity of optical fiber sensors at cryogenic temperatures *Opt. Mater. Express* **7** 1754–66
[28] Nanato N and Nishiyama K 2014 Non-destructive detection of normal transitions in high temperature superconducting coil *Proc. 26th Int. Symp. on Superconductivity (ISS 2013); Phys. Proc.* **58** 260–3
[29] Nanato N and Nishiyama K 2015 Locating of normal transitions in a Bi2223 high temperature superconducting coil by non-contact voltage measurement method *Cryogenics* **72** 53–6
[30] Ravaioli E, Martchevsky M, Sabbi G, Shen T and Zhang K 2018 Quench detection utilizing stray capacitances *IEEE Trans. Appl. Supercond.* **28** 1–5
[31] Zhang K *et al* 2018 Tripled critical current in racetrack coils made of Bi-2212 Rutherford cables with overpressure processing and leakage control *Supercond. Sci. Technol.* **31** 105009
[32] Shen T *et al* 2019 Stable, predictable and training-free operation of superconducting Bi-2212 Rutherford cable racetrack coils at the wire current density of 1000 A $mm^{-2}$ *Sci. Rep.* **9** 10170
[33] Iossel Y Y, Kochanov E S and Strunskii M G 1971 The calculation of electrical capacitance *Technical Report* Foreign Technology Div Wright-Patterson AFB OH
[34] Arp V D, McCarty R D and Friend D G 1998 Thermophysical properties of helium-4 from 0.8 to 1500 K with pressures to 2000 MPa *NIST Technical Note* 1334 National Institute of Standards and Technology
[35] Jensen J E, Brechna H, Stewart R G and Tuttle W A 1980 *Brookhaven National Laboratory Selected Cryogenic Data Notebook* (New York: Brookhaven National Laboratory)
[36] Mossotti O F 1850 Discussione analitica sull'influenza che l'azione di un mezzo dielettrico ha sulla distribuzione dell'elettricità alla superficie di più corpi elettrici disseminati in esso *Memorie di Matematica e di Fisica della Società Italiana delle Scienze Residente in Modena* vol 24
[37] Clausius R 1879 *Die Mechanische Behandlung der Electricität* (Wiesbaden: Vieweg+Teubner Verlag)
[38] Markiewicz W D, Dixon I R, Eyssa Y M, Schwartz J, Swenson C A, Van Sciver S and Schneider-Muntau H J 1996 25 T high resolution NMR magnet program and technology *IEEE Trans. Magn.* **32** 2586–9
[39] Yin S, Arbelaez D, Swanson J and Shen T 2019 Epoxy resins for vacuum impregnating superconducting magnets: a review and tests of key properties *IEEE Trans. Appl. Supercond.* **29** 7800205
[40] Kirby G A *et al* 2018 Hi-Lumi LHC twin aperture orbit correctors 0.5-m model magnet development and cold test *IEEE Trans. Appl. Supercond.* **28** 1–5
[41] Savary F *et al* 2016 11 T dipole for HL-LHC: status and plan *IEEE Trans. Appl. Supercond.* **26** 1–5
[42] Wilson M N 1983 *Superconducting Magnets* (*Monographs on Cryogenics*) (Oxford: Clarendon)
[43] Verweij A P 1995 Electrodynamics of superconducting cables in accelerator magnets *PhD Thesis* Twente U., Twente